Clay Minerals, (2017) **52**, 521–535

Preparation and catalytic activities of porous clay heterostructures from aluminium-intercalated clays: effect of Al content

FETHI KOOLI[1,*], YAN LIU[2], KAIS HBAIEB[3] AND RAWAN AL-FAZE[4]

[1] *Taibah University-Al-Mahd Branch, Community College, Al-Mahd 44412, Saudi Arabia*
[2] *Institute of Chemical and Engineering Sciences, 1 Pesek Road, Jurong Island, Singapore 627833*
[3] *Mechanical Engineering Department, Taibah University, POB 141 Madinah Al-Munawwarah, Saudi Arabia*
[4] *Taibah University, Chemistry Department, P.O. Box 30002, Al-Madinah Al-Munawwarah 41447, Saudi Arabia*

(*Received 2 July 2017; revised 5 January 2018; Associate Editor: Chris Greenwell*)

ABSTRACT: Porous clay heterostructures were prepared from Al-intercalated clays, and they allowed the insertion of Al into the framework of intercalated silica in porous clay heterostructures (PCHs). This method has led to tuneable Al contents within the resulting porous clay heterostructures. X-ray fluorescence confirmed the presence of Al in the intercalated precursors and their derivatives (porous clay heterostructure materials) in various environments, as indicated by ^{27}Al magic-angle spinning nuclear magnetic resonance. The Al porous clay heterostructures exhibited specific surface areas that varied from 743 to 850 m^2/g with total acid concentrations which varied from 0.969 to 1.420 mmol of protons/g of material, values which were deduced from the temperature desorption of cyclohexylamine. These acid sites were sufficiently strong to initiate the hydro-isomerization of n-heptane. The catalytic properties of the porous clay heterostructures depended on the Al contents and reached a maximum conversion rate of 50% and an isomer selectivity of 70% at a test reaction temperature of 350°C.

KEYWORDS: clay minerals, pillared clays, porous heterostructure clays, mesoporous materials, hydro-isomerization.

Clay minerals are of considerable interest from a research point of view. In addition to their conventional applications in catalysis, ceramics and adsorbents, new applications have emerged in the pharmaceutical industry and particularly in drug delivery (Carretero *et al.*, 2006; Lopez-Galindo *et al.*, 2007; Carretero & Pozo, 2009; Rodriguez *et al.*, 2013; Ghadiri *et al.*, 2015). Catalytic application requires particular structural and acidic stabilities at moderate and high temperatures (Adams & McCabe, 2006). Porous clay heterostructures (PCHs) were amongst the candidates for this application. These materials were synthesized from swelling clay minerals, such as montmotrillonite, and the clay layers were initially intercalated using cationic surfactants *via* a cation exchange reaction and later reacted with co-surfactant molecules (neutral aliphatic amines) and a silica precursor (such as tetraethylorthosilicate, TEOS) (Galarneau *et al.*, 1995). The hydrolysis and polymerization of silica species surrounding the template of the surfactant and co-surfactant occurred and produced a heterostructure template. After the removal of organic surfactants by calcination or treatment with an ammonium chloride solution (Galarneau *et al.*, 1995; Kooli *et al.*, 2006a,b) a porous network of silica within the interlayer region was formed. The PCHs exhibited greater specific surface areas, surface acidity, and narrow pore-size distributions in the super-micropore to mesopore range (Ahenach *et al.*, 2000; Polverejan *et al.*, 2000; Kooli *et al.*, 2006a,b).

* E-mail: fkooli@taibahu.edu.sa
https://doi.org/10.1180/claymin.2017.052.4.09

These physicochemical properties of PCH materials can be improved by changing the properties of the host clay minerals either by varying the nature of the clay minerals (Polverejan *et al.*, 2000; Palkova *et al.*, 2010; Perdigon *et al.*, 2013) or by acid activation of the parent clays prior to use (Kooli *et al.*, 2006a,b). Moreover, acid-activated clays were used as starting precursors, and the resulting PCH materials exhibited greater surface areas and acidity compared with materials that were prepared from non-acid-activated clays (Kooli *et al.*, 2006a,b). Pure mesoporous silica possesses little or no acidity (Mokaya *et al.*, 1996) and the incorporation of metal cations into the silica framework of PCHs induced extra acidic properties with the addition of the corresponding metal alkoxide (titanium or zirconium) or metal-organic C_6H_5FeO with a silica source during the preparation process (Chmielarz *et al.*, 2009; Cecilia *et al.*, 2013; Zimowska *et al.*, 2016). Another method consisted of the adsorption of the Al acetylacetonate complex followed by thermal decomposition, which resulted in Al oxide PCHs (Ahenach *et al.*, 2000).

PCH materials are considered to be pillared clays with silica pillars inserted between the clay layers depending on the preparation and mechanism used. Using this idea, a novel synthesis method was proposed by Kooli *et al.* (2006a, 2014a) which consisted of integrating intercalated Al species into clay minerals as precursors prior to reactions with C_{12} amine molecules and silica sources to prepare Al-incorporated PCH (Al-PCH) materials. These Al-PCH materials with fixed Al contents exhibited larger surface areas and mesoporous volumes, and more Brønsted and Lewis acid sites (Kooli *et al.*, 2006a,b, 2014). Similarly, Zr-intercalated clay minerals were used to incorporate zirconium species directly into the silica framework between the clay layers (Kooli *et al.*, 2016). The variation in the Zr content in Zr-PCH materials was achieved by varying the Zr species content in the parent intercalated precursors (Kooli *et al.*, 2016). This method has reduced the utilization of the organic template and, in one step, incorporated the Al or Zr species directly into the silica framework that was intercalated between the clay layers. In the present study, the effect of the Al content on the physicochemical properties, such as thermal stability, microtextural properties and acidity of the resulting PCH materials, was investigated. For this purpose, various clays with intercalated Al species were prepared at various starting mmol of Al/g of clay using Al chlorhydrate hydroxide (Chlorhydrol, 50%). Various techniques were used to characterize these materials, including *in situ* X-ray diffraction (XRD). The acidity was examined using temperature-induced desorption of cyclohexylamine molecules. Catalytic testing of the resulting Al-PCH materials was conducted in the hydroisomerization step of the n-heptane reaction.

EXPERIMENTAL

Materials

The chemicals used for the preparation of Al-intercalated clays and their PCH counterparts were purchased from Sigma-Aldrich, were of analytical grade and were used without further purification. The clay mineral (Ca-montmorillonite, STx-1) was purchased from the Source Clays Repository of The Clay Minerals Society, Purdue University (USA) with a cation exchange capacity of 92 meq/100 g. The pillaring agent solution of Al chlorhydrate hydroxide (Chlorhydrol, 50%) was provided by the Reheis Chemical Company, New Jersey, USA.

Preparation of Al-intercalated clays

A series of Al-intercalated clays was prepared using the cation exchange reaction with a solution of Chlorhydrol (50%) at various Al:clay ratios from 3 to 24. Briefly, a specific mass of Chlorhydrol solution was added to 200 mL of deionized water, which was further aged at 80°C for 1 h prior to adding 5 g of clay in dry powder form. The suspension was mixed for another 1 h and aged at 80°C. The resulting suspension was cooled at room temperature. The solid was recovered by filtration and washed repeatedly with deionized water and subsequently air-dried overnight. The samples were identified as Al(X)-Mt, where X corresponds to the Al (mmol):clay (g) ratio.

Preparation of Al-PCHs

The PCH precursor was prepared as reported previously (Kooli, 2014a). Briefly, 1 g of the Al-intercalated clay was reacted with neutral amine (dodecylamine, $C_{12}H_{25}NH_2$) and TEOS at molar ratios of clay/$C_{12}H_{25}NH_2$/TEOS of 1/20/150. The mixture was stirred for 4 h at room temperature. After the reaction, the PCH precursor obtained was recovered by filtration and air-dried overnight. The sample was designated Al(X)-PCH. The resulting Al(X)-PCH materials were obtained after calcination at 550°C for 6 h in air at a heating rate of 1°C/min. In certain cases, the temperature of calcination varied from 550 to

https://doi.org/10.1180/claymin.2017.052.4.09 Published online by Cambridge University Press

900°C for 6 h with the same heating rate of 1°C/min for a selected Al(6)-PCH precursor.

In the text, the term 'precursor' describes the as-synthesized product (intercalated), and 'material' designates the calcined precursors at various temperatures.

Preparation of Pd catalysts

The preparation of the bifunctional catalysts (with 0.5% Pd) was carried out by incipient-wetness impregnation. Then, the impregnated sample was dried at 110°C for 24 h followed by calcination at 500°C for 3 h.

Characterization

The intercalation of Al polyoxocations (Al_{13} species) between the clay layers and the successful synthesis of PCH materials was confirmed using XRD (Bruker D8 Advance Model diffractometer equipped with a Ni filter and Cu-*K*α radiation (λ = 0.15406 nm) in the range 1.5–50°2θ). The *in situ* studies were performed using an Anton Parr heating stage (KT450) which was attached to the X-ray diffractometer over the range of room temperature–425°C. The chemical composition of the intercalated clays and PCH derivatives was determined using X-ray Fluorescence (XRF) (Bruker Model S4). The samples were pressed into boric-acid pellets. The specific surface areas, pore volumes and pore-size distributions were obtained using a Micromeritics ASAP 2040. The samples were degassed under vacuum overnight at 150°C prior to analysis. The ^{29}Si solid state and solid ^{27}Al magic-angle spinning nuclear magnetic resonance (MAS NMR) spectra were collected using a Bruker spectrometer as reported elsewhere and tetramethylsilane (TMS) as reference for the zero chemical shift. Thermogravimetric analysis (TGA) features were obtained after experiments using the TA Instruments model 9610 under atmospheric air and a heating rate of 10°C/min. The same machine was used to estimate the acidity employing cyclohexylamine as a probe molecule. The hydro-isomerization tests of n-heptane were conducted in a microreactor that was connected to a gas chromatography (GC) line, as reported in a previous study (Liu *et al.*, 2006a,b).

RESULTS AND DISCUSSION

XRF data

Chemical analyses of the Al-intercalated precursors and their resulting PCH derivatives are presented in Table 1. The quantity of Al intercalated in the precursors depended on the starting ratios of Al (mmol):clay (g). The largest amount of Al was intercalated at a ratio of 6 mmol of Al/g of clay. The cation exchange reaction resulted in a further reduction in Ca^{2+} ions, which were completely removed for ratios of Al mmol/g of clay that were >6:1 (Kooli *et al.*, 2016). An increase in Al_2O_3 oxide was accompanied by a decrease in SiO_2 and other oxide contents. The chemical analysis indicated that the ratios of mmol of Al/g of clay were smaller than the starting ratio (Table 1). Similar data were reported for other clay minerals using the same Al pillaring agent (Kooli & Jones, 1997).

As expected, after reactions with TEOS and dodecylamine, the resulting PCH materials exhibited greater SiO_2 contents than the starting precursors because of the addition of a silica source during the preparation of PCH precursors and a decrease in the contents of the other oxides, especially Al_2O_3. This decrease can be related to the exchange of several intercalated Al species with the C12 amine, as reported previously (Kooli, 2014a,b). The percentage of Al in PCH materials varied over the range 4.3–6.4%. These values were within the range (4–8%) reported previously for other Al-PCH materials prepared by various methods (Zimowska *et al*. 2016), thereby confirming the benefit of using different precursors.

X-ray diffraction

Powder XRD patterns of montmorillonite (Mt) that was exchanged with various intercalated quantities of Al species are presented in Fig. 1. The raw clay (Mt) pattern is shown for comparison (Fig. 1a). The precursor Al(*X*)-Mt exhibited an increase in terms of the basal spacing (deduced from the 001 reflection) from 1.52 nm to larger values, which depended on the starting Al to clay ratios. The increase in the basal spacing was related to the amount of Al polyoxocationic species intercalated, and varied from 1.91 nm for Al(3)-Mt (Fig. 1b) to 2.39 nm for Al(6)Mt (Fig. 1c). A slight variation from 2.39 to 2.35 nm and 2.32 nm was observed for Al(12)-Mt and Al(24)-Mt (Fig. 1d,e), respectively, which can be related to a minor decrease in Al content. Taking into account the 0.96-nm thickness of the Mt layers themselves (Brindley & Hoffmann, 1962), the Al(*X*)-Mt precursors exhibited an interlayer spacing which varied from 0.89 to 1.20 nm. The values obtained were close to the size of Al_{13} polyoxocations, as reported in the literature (Kloprogge, 1998). The reflection at 0.41 nm that

https://doi.org/10.1180/claymin.2017.052.4.09 Published online by Cambridge University Press

TABLE 1. Chemical analysis (major elements, mass %) of Al(*X*)-Mt and their PCH derivatives.

Samples	SiO_2	Al_2O_3	MgO	Fe_2O_3	CaO	TiO_2	K_2O	Al_2O_3[a]	Al/clay[b]
Mt(0)-Al	72.2 (74.2)	14.5 (13.5)	3.09 (2.66)	0.884 (0.66)	1.77 (0.96)	0.236 (0.20)	0.108 (0.091)	0.00	0
Mt(3)-Al	60.1 (76.2)	16.7 (4.3)	2.95 (2.42)	0.745 (0.62)	0.45 (0.61)	0.124 (0.16)	0.084 (0.075)	8.56	1.67
Mt(6)-Al	55.0 (80.1)	20.2 (6.4)	2.43 (0.61)	0.489 (0.14)	0.05 (0.02)	0.019 (0.03)	0.062 (0.03)	12.01	2.35
Mt(12)-Al	54.1 (81.5)	18.1 (5.5)	1.95 (0.50)	0.325 (0.12)	0.041 (0.02)	0.019 (0.03)	0.062 (0.03)	10.26	2.01
Mt(24)-Al	52.2 (81.9)	17.1 (5.8)	2.01 (0.56)	0.412 (0.14)	0.041 (0.02)	0.019 (0.03)	0.062 (0.03)	9.31	1.82

Values in parentheses correspond to the resulting PCH materials.
[a]Corresponds to Al_2O_3 content in the intercalated clays.
[b]Corresponds to experimental mmol of Al:clay ratios

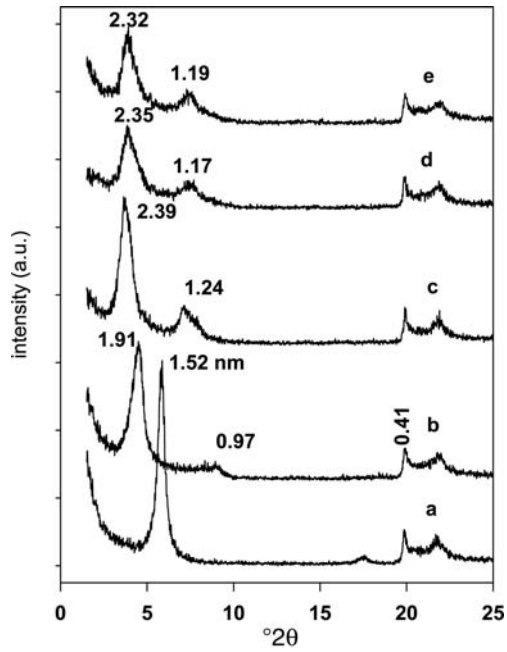

FIG. 1. Powder XRD patterns of Mt clay exchanged with Al polyoxocations at different ratios (R) of mmol of Al/g of clay: (a) R = 0, (b) R = 3, (c) R = 6, (d) R = 12 and (e) R = 24.

corresponded to the 110 reflection was observed (Fig. 1), which indicated that the layered structure was not severely altered (Kooli *et al.*, 2014).

After reaction with TEOS and C_{12}-amine molecules, the basal spacing of raw Mt increased slightly from 1.52 to 1.70 nm (Fig. 2a); however, it further expanded to values that varied from 3.61 nm (for Al(3)-PCH, Fig. 2b) to 4.10 nm (for Al(12)-PCH, Fig. 2d), which depended on the type of Al(*X*)-Mt precursors (Fig. 2c,d). These values were close to those reported for similar PCH precursors (Tchinda *et al.*, 2009; Garea *et al.*, 2014). After calcination at 550°C, the basal spacing of the material that was obtained from pure Mt (Al(0)-PCH) decreased from 1.70 to 1.14 nm (Fig. 2a′). This value was greater than that reported for totally collapsed clay (0.96 nm). This variation can be related to the presence of silica species or organic materials (Kooli, 2014a,b). For the other materials, a shrinkage of the basal spacing was observed (Fig. 2b′–e′), which was due to surfactant combustion and the formation of three-dimensional silica species, as reported for PCH materials that were prepared using conventional methods (Tchinda *et al.*, 2009). The powder XRD patterns exhibited only reflections at low

https://doi.org/10.1180/claymin.2017.052.4.09 Published online by Cambridge University Press

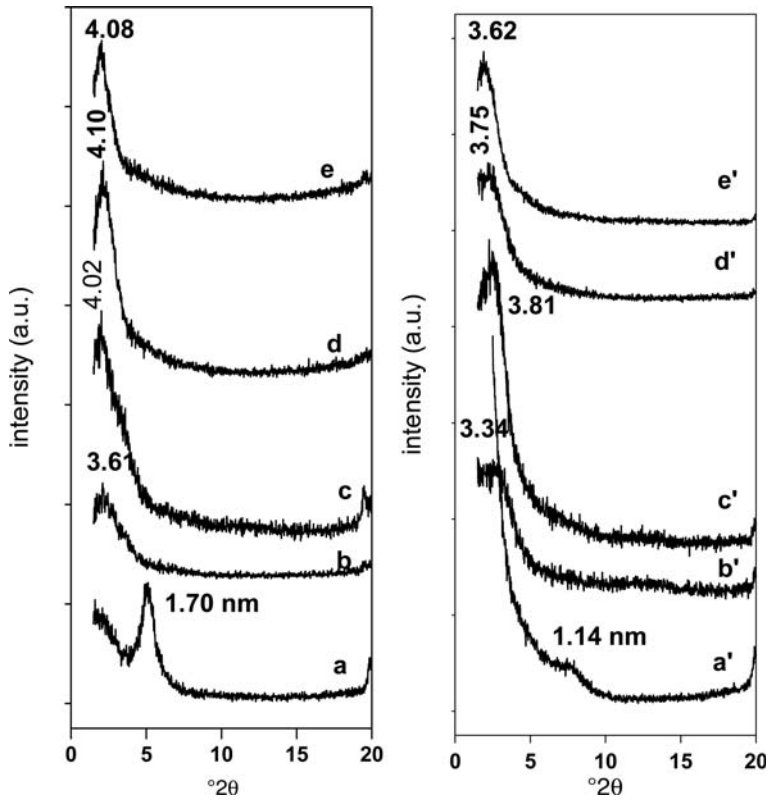

FIG. 2. Powder XRD patterns of Al(*X*) PCH precursors that were prepared from Al polyoxocation-intercalated clays at different ratios (R) of mmol of Al/g of clay: (a, a′) R = 0, (b, b′) R = 3, (c, c′) R = 6, (d, d′) R = 12 and (e, e′) R = 24 before and after (prime) calcination at 550°C.

2θ angles, and no multiple reflections were detected, consistent with similar data reported in the literature (Tchinda *et al.*, 2009). The smaller value of 3.34 nm was obtained for Al(3)-PCH (Fig. 2b′), and a larger value of 3.81 nm was obtained for Al6-PCH (Fig. 2c′). The other two materials exhibited intermediate values of the basal spacing of 3.75 and 3.62 nm, respectively (Fig. 2d′,e′). This method has enabled the tuning of the basal spacing in PCH.

Solid ^{29}Si and ^{27}Al NMR

The presence of silicon species in synthesized PCH materials was confirmed using solid ^{29}Si NMR. The solid ^{29}Si NMR spectrum of the raw Mt clay exhibited two resonance peaks at −95.6 and −111.8 ppm (Fig. 3a). The first peak (at −95.6 ppm) was assigned to Si atoms that were linked through oxygen to three other Si atoms and to one Al or (Mg) atom in the octahedral sheet. The second resonance at 111.8 ppm was due to amorphous silica impurities, which were present in the raw clay (Fig. 3a, Kooli *et al.*, 2005). Upon intercalation of the Al pillaring agent, the solid ^{29}Si NMR spectra of the resulting clays were similar to that of the parent Mt with a slight variation in the peak position, which indicates that the layered structure was not altered during the cation exchange reaction (an example for Al(6)-Mt is presented in Fig. 3b). These data are in good agreement with the XRD data and other cation exchange reactions with Zr species (Kooli *et al.*, 2016). The solid ^{29}Si NMR spectra of the resulting Al porous heterostructure precursors were different and exhibited additional resonance peaks due to the presence of intercalated silica species. The Al(6)-PCH spectrum is shown as a representative one (Fig. 3c), which exhibited an intense resonance peak at −110.8 ppm and a weak peak at −100.2 ppm (Tchinda *et al.*, 2009; Wang *et al.*, 2016). The spectrum did not display the characteristic resonance peak of TEOS at −81.7 ppm, which confirms the

https://doi.org/10.1180/claymin.2017.052.4.09 Published online by Cambridge University Press

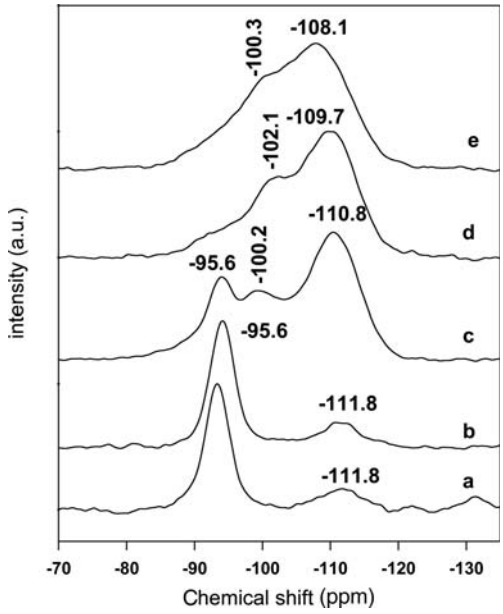

FIG. 3. Solid ^{29}Si NMR spectra of: (a) Mt clay, (b) exchanged with Al polyoxocations at a ratio of 6 mmol of Al/g of clay; (c) then reacted with C12 amine and TEOS solutions; (d) and (e) correspond to sample (c) after calcination at 550°C and 750°C, respectively.

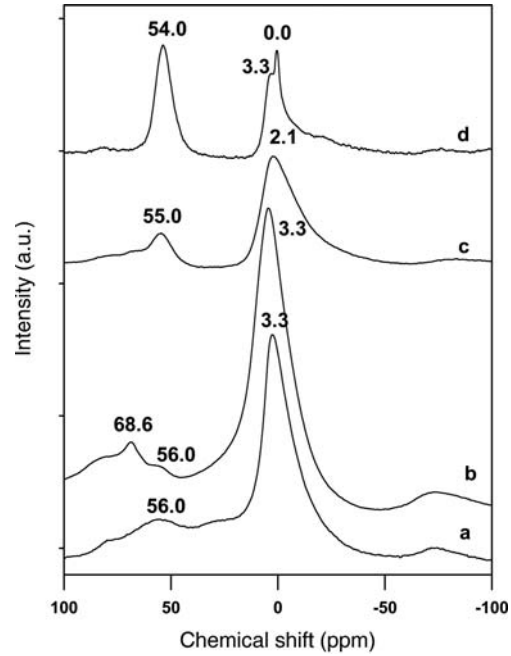

FIG. 4. Solid ^{27}Al MAS NMR spectra of: (a) Mt clay, (b) exchanged with Al polyoxocations at a ratio of 6 mmol of Al per g of clay (Mt); (c) then reacted with C12 amine and TEOS solutions; (d) corresponds to sample (c) calcined at 550°C.

polycondensation of silicon species (Belver *et al.*, 2012). The peaks at −110.8 and −100.2 ppm were assigned to Q^4 Si species Si(SiO_4) and Q^3 Si species (HO)(SiO_3), respectively (Ghanbari-Siahkali *et al.*, 2000; Perdigon *et al.*, 2013). The solid ^{29}Si NMR resonance peak of the octahedral sheet at −95.6 ppm was observed with lower intensity due to the high intensity of the peak at −110.8 ppm (Fig. 3c). The precursors that were prepared from other Al(*X*)-Mt materials exhibited similar features and the positions of the resonance peaks that were related to the intercalated silica species were unchanged (not shown). Upon calcination at 550°C, the resonance peak of Q^4 Si species became broad and shifted to a smaller value of −109.7 ppm due to dehydroxylation of intercalated silica species (Fig. 3d, Kooli *et al.*, 2014). The Q^3 Si peak at −95.6 ppm (related to the clay layers) decreased in intensity and became broader, with a shift to −92.5 ppm (Fig. 3d) whereas the peak related to Q^3 mesoporous silica remained observable with a slight shift in position to −102.1 ppm (Fig. 3d). The spectrum features were maintained after calcination at 650°C (not shown). Similar data were also reported for Zr-PCH materials (Kooli *et al.*, 2016), and the spectra mainly exhibited a broad resonance peak at ∼−108.1 ppm, which is related to the Q^4Si species with two different shoulders. The broadness of the resonance peaks may be due to the coexistence of different Si species that were mixed in one phase. The peak related to the clay layers or other silica species were difficult to detect, particularly at 750°C or greater (Fig. 3e). In the case of mesoporous silica materials that were doped with different cations, several doublets have been reported previously and associated with their insertion in the silica framework (Choy *et al.*, 2004). In our case, it was difficult to detect such doublets due to the broadness of the peaks and their overlap.

The aim of using solid state ^{27}Al MAS NMR was to confirm the presence of Al species in their environments compared with intercalated Al(*X*)-Mt precursors. The spectrum of the raw Mt clay, which is presented in Fig. 4a, exhibited two clear signals at 3.3 and 56.0 ppm, which correspond to Al in an octahedral environment and 4-coordinated Al that substituted for the silica in the tetrahedral sheets, respectively (Thompson, 1984). The presence of the intercalated Al species in Al(*X*)-Mt precursors exhibited broad

https://doi.org/10.1180/claymin.2017.052.4.09 Published online by Cambridge University Press

characteristics of Al peaks with an additional peak between 60 and 70 ppm (at 68.6 ppm) which was assigned to tetrahedral Al from the pillaring species, as reported in the literature (Fig. 4b represents the spectrum related to Al(6)-Mt precursor, González *et al*. 2009). The solid ^{27}Al MAS NMR data confirmed the presence of the Al species in Al(*X*)-PCH precursors, Fig. 4c represents the spectrum of the Al(6)-PCH precursor. After calcination at 550°C, for example, the spectrum of Al(6)PCH material exhibited two signals at 0.0 and 3.3 ppm (Fig. 4d), however, which relate to the presence of Al in two environments, and which can be associated with 4-coordinated Al in the parent clay layers and Al that was inserted in the silica framework of the PCH material. In addition, an improvement in the signal at 54.0 ppm was also observed (Fig. 4d). This feature was comparable to that reported for similar Al-PCH materials (Kooli *et al.*, 2006a,b, 2014).

TGA data

Thermogravimetric analysis (TGA) was performed in order to study the thermal properties of the parent clays and the resulting materials after the pillaring process and PCH synthesis. These data were reported in terms of derivative thermogravimetric analysis (DTG). This mathematical transformation was used to identify the maximum temperature in a loss step and to differentiate between the overlapping steps in terms of the mass loss (Kooli *et al.*, 2014). The TGA of the parent clay with a total mass loss of 24% occurred over several ranges of temperature. In the first range, dehydration occurred in two steps between 25 and 100°C and between 100 and 200°C, which correspond to the loss of water that was physically adsorbed on the surface and water molecules that were in contact with the cations in the interlayer region, respectively (Borges *et al.*, 2016). The DTG curve exhibited two maximum temperatures of loss at 70 and 140°C (Fig. 5a). The region between 500 and 850°C recorded a loss of 6.8% in mass with a linear tendency with respect to temperature, which is attributed to dehydroxylation of the clay layers with a DTG peak at 655°C (Fig. 5a, Kooli *et al.*, 2014). The DTG curve of Al-intercalated clays exhibited two peaks at 53 and 70°C (an example for Al(3)-Mt and Al(6)-Mt precursors are presented in Fig 5b,c, respectively) related to the loss of different types of water molecules. A broad signal at ~147°C was also observed, and it was related to intercalated water molecules. A significantly greater quantity of water was present in the intercalated materials compared with the parent clay (Kloprogge *et al.*, 1994). The continuous mass loss that was observed in the range of 240–900°C was attributed to water molecules that were coordinated with the pillars and the dehydroxylation of the pillars and clay layers. The DTG curve exhibited a broad peak at 580°C (Fig. 5b,c). It was difficult to distinguish between these steps due to their overlap. The mass loss between 25 and 900°C in Al(*X*)-Mt precursors depended on the amount of pillaring species and was greater than that of the parent clay. The maximum temperature that was related to the dehydroxylation process was less than that of the parent clay mineral. Similar observations were noted for the presence of inorganic or organic pillaring species (Kooli, 2014a,b; Kooli *et al.*, 2014). However, the DTG curves of Al(*X*) PCH precursors exhibited different features and additional peaks in the range 200–400°C were due to the presence of C_{12} amine surfactants (*e.g.* DTG curves of Al(3)-PCH and Al(6)-PCH are presented in Fig. 5b′,c′, Kooli *et al.*, 2014; Wang *et al.*, 2016). The presence of C_{12} amine molecules reduced the mass loss of water molecules at low temperatures, and only a 5% mass loss was recorded with a low-intensity DTG peak at 50°C

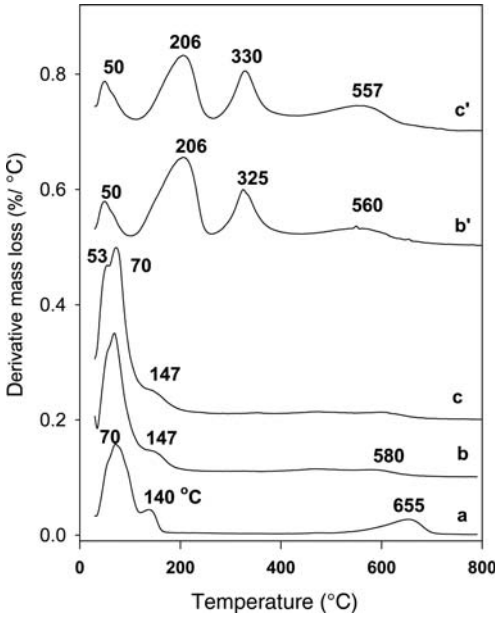

FIG. 5. DTG features of: (a) Mt clay exchanged with Al polyoxocations at (b) a ratio of 3 mmol of Al/g of clay and (c) at a ratio of 6 mmol of Al/g of clay. b′ and c′ correspond to samples b and c reacted with C_{12} amine and TEOS solutions, respectively.

https://doi.org/10.1180/claymin.2017.052.4.09 Published online by Cambridge University Press

(Fig. 5b′,c′, Kooli, 2014a,b). The loss of organic molecules occurred in two steps at temperatures of 206 and 325°C for Al(3)-PCH and at 330°C for Al(6)-PCH precursors (Fig. 5b′,c′). The dehydroxylation of intercalated silica species was difficult to observe because of overlap with the DTG peaks. The maximum temperature of the mass loss in the range 350–600°C continued to decrease and shifted to 557–560°C (Fig. 5b′,c′). A slight shift in the maximum temperature was observed which was related to the mass loss of water, organic surfactants and dehydroxylation of clay layers.

Thermal stability

In this case, *in situ* XRD was used, and the patterns were recorded at the actual temperature without cooling the sample. The treatment of the parent Mt clay at temperatures in the range 25–420°C indicated that the basal spacing (deduced from the first (001) reflection) decreased continuously from 1.53 (Supplementary material Fig. S1a, http://www.minersoc.org/pages/e_journals/dep_mat_cm.html) to 0.98 nm (Fig. S1e) whilst passing through intermediate values of 1.40 nm (Fig. S1b), 1.18 nm (Fig. S1c) and 1.03 nm (Fig. S1d) at 50, 100 and 150°C, respectively. Above 150°C, the basal spacing contracted slightly from 1.03 to 0.98 nm and was accompanied by a loss in the crystal order, which is indicated by an intensity decrease in the first reflection (Fig. S1e). The decrease in the basal spacing was associated with the loss of the first and second layers of water molecules and was also in good agreement with the TGA data (Wilson *et al.*, 2004; Kooli, 2014a,b).

In the case of Al-intercalated precursors, Al(6)-Mt was selected and the related *in situ* XRD data are presented in Fig. 6. The basal spacing of the Al(6)-Mt decreased from 1.90 to 1.87 nm at 150°C (Fig. 6a,b) with an improvement in the crystal order with detection of multiple reflections of 00*l*. Above 200°C, a slight variation in the crystal order was observed, and the basal spacing remained close to 1.86 nm (Fig. 6c–f). This value of 1.86 nm was greater than the 0.98 nm value of the parent clay due to the presence of the pillaring species that prevented the collapse of the layers. The *in situ* data indicated that calcination at 200°C is sufficient to produce a stable material, and this value was lower than that reported in the literature for producing pillared clays at temperatures of >400°C (Jones, 1988; Schoonheydt *et al.*, 1999).

The *in situ* data for the Al(6)-PCH precursor calcined at different temperatures are depicted in Fig. 7. The basal spacing of the precursor did not vary at 150°C (Fig. 7a,b); however, it decreased starting from 200°C (Fig. 7c) due to release of organic surfactants, as indicated by the TGA data. The basal spacing continued to decrease slightly up to 3.76 nm at 425°C at calcination temperatures of 300, 400 and 425°C (see Fig. 7d–f). This value (425°C) was the maximum temperature attained with the Anton Parr cell used in the present study. The calcination of the precursor in air (*ex situ*) at 400 and 550°C led to a stable material with clear reflections at 3.75 and 3.81 nnm, respectively (Fig. S2). At increasing temperatures, the intensity of the first peak disappeared at 650°C due to a decrease in crystal order. Further calcination at >650°C led to a similar material, and no reflections were recorded at lower angles; an example is presented after calcination at 750°C (Fig. S2).

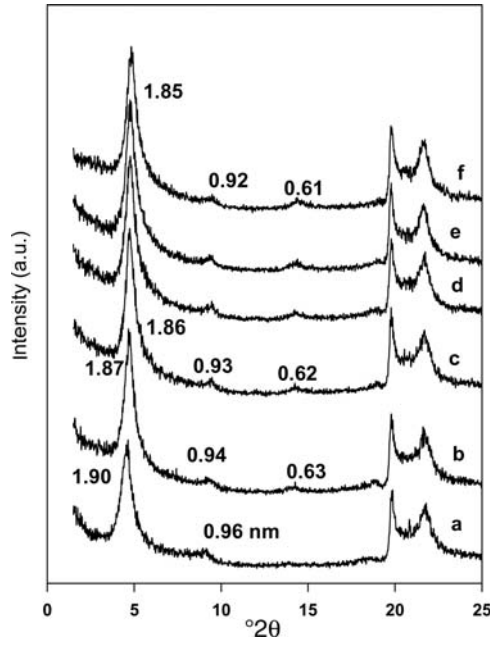

FIG. 6. *In situ* powder XRD patterns of Mt exchanged with Al species at a ratio of 6 mmol of Al/g of clay and calcined at various temperatures: (a) 25, (b) 150, (c) 200, (d) 300, (e) 400 and (f) 425°C.

Microtextural properties

The isotherm of pristine Mt clay that was calcined at 550°C was a type IV characteristic of non-porous materials with a large hysteresis loop (Fig. 8a) (Wang *et al.*, 2016). The pillaring materials (obtained after

https://doi.org/10.1180/claymin.2017.052.4.09 Published online by Cambridge University Press

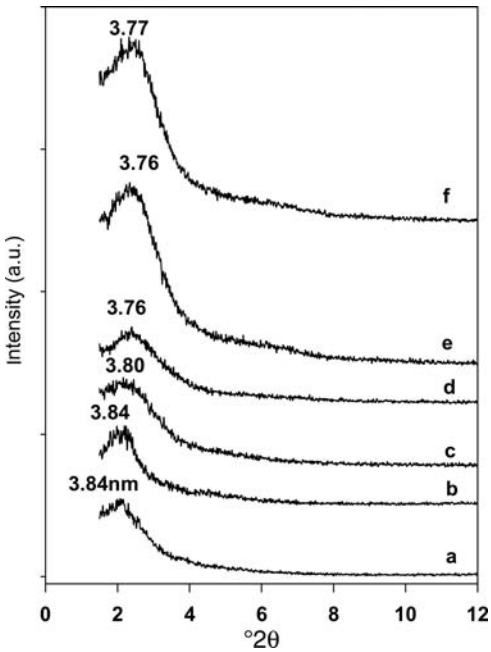

FIG. 7. *In situ* powder XRD patterns of Mt exchanged with Al species at a ratio of 6 mmol of Al/g of clay after reaction with C_{12} amine and TEOS solutions (Al(6)-PCH precursor), calcined at various temperatures: (a) 25, (b) 150, (c) 200, (d) 300, (e) 400 and (f) 425°C.

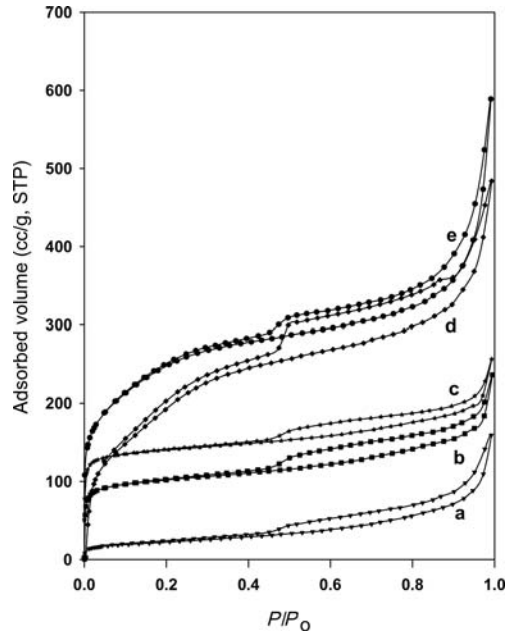

FIG. 8. Nitrogen adsorption-desorption isotherms of: (a) Mt, (b) Al(6)-Mt, (c) Al(3)-Mt calcined at 550°C, (d) Al(3)-PCH and (e) Al(6)-PCH precursor calcined at 550°C.

calcination at 550°C) exhibited different shapes between type I and type IV. The shapes were close to type I in the low relative-pressure region, indicating the presence of micropores, and type IV at higher relative pressures (a representative isotherm is reported in Fig. 8b for Al(6)-Mt). An increase in the adsorbed volume at lower temperatures was observed due to the increase in interlayer space compared with the parent Mt (Fig. 8c, Kooli *et al.*, 2014, 2016).

The shape of the calcined Al(*X*)-Mt was not changed with respect to the Al quantity that was present in pillared clays. There was a slight decrease in the volume adsorbed at lower relative pressures, however, due to the decrease in alumina content (Fig. 8b,c). Similar shapes were reported for other pillared materials (Martinez-Oritz *et al.*, 2003). The shape of hysteresis corresponded to type IV, which is related to the formation of mesopores between the interlayers. The starting clay had a surface area of 90 m^2/g. The incorporation of alumina species between the layers was accompanied by an increase in the surface area from 90 to 321 m^2/g, which depended on the quantity of alumina (Table 2). The highest value was obtained for Al(3)-Mt and the lowest value was achieved for Al(24)-Mt. The percentage increase in the micropore surface area was in the range 52–65%, and the micropore volume depended on the amount of Al intercalated, which varied from 0.102 to 0.067 cm^3/g. Thus, the percentage of pore volume from the presence of micropores was in the range 30.21–39.38%. The average pore diameter in the starting clay was ~5.81 nm which decreased after pillaring and indicated that pillared clays had mesoporous characteristics (Kooli *et al.*, 2014).

Al(*X*)-PCH materials (after calcination at 550°C) exhibited different isotherm shapes (Figs 8d and 8e correspond to Al(3)-PCH and Al(6)-PCH materials, respectively), which were close to those reported for conventional PCH materials with type IV characteristics and suggest greater porosity and a hysteresis loop that is typical of open cylindrical pores at both sides (Pichowicz & Mokaya, 2001; Kooli *et al.*, 2006a,b, Wang *et al.*, 2016). The Al(*X*)-PCH isotherms exhibited a significant increase in nitrogen adsorbed at low to medium relative pressures, which indicates the easy accessibility of nitrogen molecules to the micropores and may suggest the presence of supermicropores and small mesopores (Galarneau *et al.*, 1995; Benjelloun *et al.*, 2002, Fig. 8d,e).

https://doi.org/10.1180/claymin.2017.052.4.09 Published online by Cambridge University Press

TABLE 2. Specific surface areas (S_{BET}), total pore volume (TPV) and average pore diameter (APD) of the Al-intercalated clays and Al(X)-PCH materials after calcination at 550°C.

Samples	S_{BET} (m^2/g)	µpore volume[a]	TPV (cc/g)	APD (nm)
Al(0)-Mt	90 (180)	0.00 (0.008)	0.138 (0.028)	5.81 (6.22)
Al(3)-Mt	321(743)	0.102 (0.000)	0.259 (0.633)	3.23 (3.40)
Al(6)-Mt	281 (850)	0.083 (0.000)	0.262 (0.851)	3.66 (3.82)
Al(12)-Mt	258 (820)	0.074 (0.000)	0.221(0.801)	3.62 (3.32)
Al(24)-Mt	247(809)	0.067 (0.000)	0.223 (0.784)	3.51(3.25)

Values in parentheses correspond to the resulting PCH materials.
[a] µpore volume = micropore volume (m^2/g).

The greater adsorption volume observed for these materials was due to capillary condensation and a possible change in the pore shapes between the particles, which is indicated by the hysteresis loop.

From the data reported in Table 2, Al(X)-PCH materials (after calcination at 550°C) exhibited greater specific surface areas which varied from 743 to 850 m^2/g. These values were greater than those of PCH materials which were prepared using conventional methods and were smaller than those of Zr-PCH materials that were prepared with similar methods (Tchinda *et al.*, 2009; Chmielarz *et al.*, 2011; Kooli *et al.*, 2016). The largest value, 850 m^2/g, was obtained for Al(6)-PCH, whereas the smallest value was attained for Al(3)-PCH (743 m^2/g). Al(X)-PCH materials did not display microporous volume which decreased dramatically to values close to zero. This finding related only to Al-modified PCH, not to Zr-modified PCHs, in which certain microporosity characteristics were preserved (Kooli *et al.*, 2016). The increase in specific surface area was accompanied by an increase in the total pore volume varying from 0.851 to 0.633 cc/g. The average pore diameters were in the range 3.82–3.25 nm, which confirmed the mesoporous characteristics of these materials.

For a selected Al(6)-PCH precursor that was calcined at various temperatures, N_2 adsorption data indicated that the Al(6)-PCH precursor exhibited a specific surface area of 441 m^2/g and pore volume of 0.357 cc/g. As mentioned above, the removal of surfactant molecules led to an improvement of S_{BET} from 441 to 508 m^2/g at 300°C. Further increases in calcination temperature resulted in surface area improvements to 850 m^2/gm due to the complete removal of residual organic surfactants as indicated by the DTG curve. This value was decreased to 795 m^2/g at 650°C; however, it reduced dramatically to 653 and 529 m^2/g after treatments at 750 and 900°C, respectively (Table 3). The PXRD patterns did not exhibit a clear reflection at lower angles for materials that were calcined at higher temperatures, as presented in Supplementary Information 2; however, larger specific surface-area values were obtained compared with those for the raw clay. The pore volume of the calcined

TABLE 3. Specific surface areas (S_{BET}), total pore volume (TPV) and average pore diameter (APD) of Al(6)-PCH materials calcined at various temperatures.

Samples	S_{BET} (m^2/g)	TPV (cc/g)	APD (nm)
Al(6)-PCH	441	0.357	3.23
Al(6)-PCH (300)*	508	0.446	3.81
Al(6)-PCH (550)*	851	0.851	3.82
Al(6)-PCH (650)*	795	0.651	3.37
Al(6)-PCH (750)*	653	0.530	3.24
Al(6)-PCH (900)*	529	0.499	3.78

*Values in parentheses correspond to the calcination temperature (°C).

https://doi.org/10.1180/claymin.2017.052.4.09 Published online by Cambridge University Press

TABLE 4. Acidity concentration (mmol of protons/g of samples) of Al-intercalated clays and their Al(X)-PCH derivatives after calcination at 550°C.

Samples	Total acidity	Weak acidity (100–310°C)	Strong acidity (310–420°C)
Al(0)-Mt	0.573	- - - -	- - - -
Al(3)-Mt	0.591 (1.320)[a]	- - - -(0.872)	- - - - (0.626)
Al(6)-Mt	0.539 (1.420)	- - - - (0.626)	- - - - (0.591)
Al(12)-Mt	0.504 (1.084)	- - - - (0.542)	- - - - (0.542)
Al(24)-Mt	0.468 (0.969)	- - - - (0.471)	- - - - (0.498)

[a]Values in parentheses correspond to the resulting PCH materials.
- - - -: not determined

materials were reduced to 30%, and the mesoporous characteristic was preserved with an average pore diameter of 3.50 nm. Similar data were reported for Zr-PCH materials that were calcined at various temperatures (Kooli *et al.*, 2016).

Acidity studies

The cyclohexylamine probe molecules were used to measure accessible acid sites that were sufficiently strong to interact with this base. Assuming that each base molecule interacts with one acid site, the mass loss between 290 and 420°C was computed to estimate the acidity in terms of millimoles of cyclohexylamine per gram of material (Breen, 1991). These data related to Al(X)-Mt are presented in Table 4. The number of acid sites in the different materials depended on the alumina content. Al(3)-Mt exhibited greater acidity, 0.591 mmol/g, at low alumina loading compared with Al(24)-Mt (0.468 mmol/g). The results were surprising and indicated that the high acidity was related to the remaining exchangeable cations in pillared clays (Breen *et al.*, 1995). In fact, the starting Mt that calcined at 550°C exhibited a relatively high acidity of 0.573 mmol/g. These values were close to those reported for pillared clays using the same Al sources or species, such as zirconia or titania (Mokaya & Jones, 1995; Kooli *et al.*, 1997, 2016).

The DTG curves of cyclohexylamine desorption exhibited mainly one peak for the mass loss at a maximum temperature of 338°C for Al(6)-Mt-, Al(12)-Mt- and Al(24)-Mt-pillared clays (an example is presented for Al(6)-Mt in Fig. 9c). However, this peak shifted to lower temperatures of 315°C for Al(3)-Mt material (Fig. 9b) and 307°C for raw Mt-calcined clay (Fig. 9a). The temperature values provided information regarding the interaction between the probe molecules and acid sites. The DTG curve for cyclohexylamine desorption from the Al(6)-PCH material was different from that of pillared clays. They exhibited two resolved peaks for mass losses at maximum temperatures of 195 and 347°C (Fig. 9f), which were associated with acid sites with different strengths. The first peak was related to weak acid sites, and the second peak was associated with base molecules that interacted with medium and strong acid sites (Kooli, 2014a,b, 2016). The first peak in the DTG curve at 195°C was proposed by different authors to be related to the acid sites that originated from

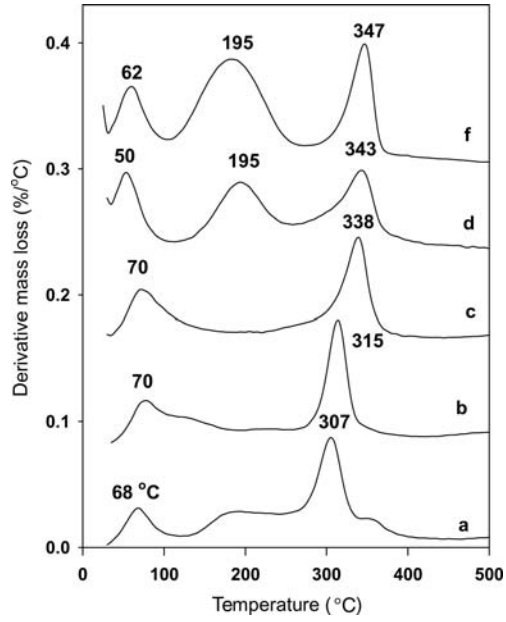

FIG. 9. DTG curves of cyclohexylamine adsorbed on: (a) Mt, (b) Al(3)-Mt, (c) Al(6)-Mt, (d) Al(3)-PCH and (f) Al(6)-PCH materials calcined at 550°C.

https://doi.org/10.1180/claymin.2017.052.4.09 Published online by Cambridge University Press

clay layers (Polverejan *et al.*, 2000; Pichowicz & Mokaya, 2001). However, in our case, the parent clay that calcined at 550°C exhibited a mass loss at a maximum temperature of 307°C, as mentioned in Fig. 9a. The peak at 50–70°C was associated with the loss of physisorbed water and base molecules. Similar DTG features were recorded for PCH materials that were prepared from Zr-intercalated clays.

The total acid content of Al(*X*)-PCH (reported in Table 4) was greater than those of pillared materials and those reported for other PCH materials that were prepared by conventional methods. This variation can be related to the contribution of the weak acid sites or the presence of Al in PCH materials. In fact, the acidity of MCM-41 (pure mesoporous silica) increased when doped with Al species (Mokaya *et al.*, 1996). The acidity variation in Al(*X*)-PCH materials was related to the reduction in the population of weak acid sites in the temperature range of 200–310°C, as shown in Fig. 9d for Al(3)-PCH material.

Hydro-isomerization catalytic properties

The transformation of aliphatic chains with carbon numbers of 5–7 was considered an important reaction in the preparation of clean fuel with improved octane numbers (Hidalgo *et al.*, 2014). This process is called hydro-isomerization and requires bifunctional metal/acid catalysts. The hydrogenation and dehydrogenation steps occur on metallic sites, whereas the isomerization or cracking steps occur on acid sites. Hence, the activity and selectivity of metal/acid catalysts depend on the characteristics of the acid sites and metallic sites (Deldari, 2005). In the present case, palladium was selected as the metal catalyst due its good activity for the reaction (Deldari, 2005).

The starting Pd-Mt clay that was calcined at 500°C (Pd-Mt(500)) exhibited low activity due to the lack of acid sites necessary for this reaction, even though it exhibited the highest acidity using cyclohexylamine, which indicates that these acid sites were not sufficiently strong for this type of reaction (Kooli *et al.*, 2008). In addition, mainly Lewis sites were detected by pyridine probe molecules (Kooli, 2014a, b). However, Pd-pillared clays (Pd-Al(*X*)Mt calcined at 550°C) exhibited improved activity compared with Pd-Mt(500) and can be related to the presence of Brønsted acid sites in the catalysts (Table 5). This activity depended on the test temperature and lower conversions between 2 and 5% were achieved at temperature of 250°C. At a test temperature of 350°C, the conversion was enhanced and reached a maximum

TABLE 5. Catalytic activities of Al-pillared clays and their Al(*X*)-PCH derivatives after calcination at 550°C.

	Conversion (%)			Selectivity (%)			Cracking (%)		
	250°C	300°C	350°C	250°C	300°C	350°C	250°C	300°C	350°C
Mt	0.0	2	4	ng	ng	ng	ng	ng	ng
Al(3)-Mt	2(3)	12(10)	21(31)	70 (80)	60(68)	45(54)	12(8)	23(24)	50(43)
Al(6)-Mt	3(2)	15(18)	34(50)	79(80)	74(62)	60(70)	15 (3)	28(20)	42(33)
Al(12)-Mt	2(3)	14(19)	30(42)	73(79)	70(82)	53(59)	13 (3)	24(18)	46(36)
Al(24)-Mt	2 (3)	13 (15)	28(36)	69(72)	65(69)	50(56)	14 (5)	27(21)	43(35)

Values in parentheses correspond to the catalytic activities of resulting PCH materials.
ng: negligible

https://doi.org/10.1180/claymin.2017.052.4.09 Published online by Cambridge University Press

of 34% for Al(6)-Mt pillared clay. This improvement in catalytic tests with temperature was reported in the literature and resulted in the activation of acid sites that were responsible for this reaction (Olaya *et al.*, 2009). The alumina content in Al(*X*)-Mt-pillared clays also affected the conversion percentages. Al(6)-Mt exhibited the greatest activity of 34%, whereas Al(3)-Mt exhibited a relatively low activity of 21%. The percentage selectivity for various tested clays decreased as the test temperature increased from 300 to 350°C, and reached a maximum of 74% for Pd-Al (6)-Mt catalysts at 300°C. Similar data were reported for other alumina-pillared materials (Kooli *et al.*, 2008, 2016; Kooli, 2014a,b). The amount of alumina in Al(*X*)-Mt-pillared clays affected the percentage of isomerization in the test reactions and especially at 350°C. This effect could be explained partially by the variation in the concentration of the acid sites as presented in Table 4. The cracking yield at a test reaction of 350°C varied from 42 to 50% and can be related to the formation of carbon species that affected the activity of the acid sites (Table 5).

The Al(*X*)-PCH materials exhibited the highest catalytic conversion and reached a value of 50% at a temperature of 350°C for the Al(6)-PCH material, with selectivity and cracking yields of 70% and 33%, respectively (Table 5). This enhancement in the conversion can be related partially to the improvement in the acid sites in the tested catalysts which were composed of relatively strong Brønsted and Lewis acid sites that were reported in pyridine desorption studies and their dispersion on the catalysts' large surface areas. In addition, the greater surface areas of the PCH materials are assumed to cause good dispersion of Pd metals and thus good activity. Compared with zeolite catalysts, the conversion of Al(*X*)-PCH materials was less because of the strength of the acid sites and pore shapes of the catalysts (Yenfeng *et al.*, 2005; Liu *et al.*, 2006a,b).

The isomerization to cracking percentage (I/C) ratio was used as an indication of the efficiency of the catalysts in this type of reaction (Eswaramoorthi *et al.*, 2003; Kooli *et al.*, 2008). For a test reaction at 300°C, the I/C ratios for Al(*X*)-Mt-pillared clays were in the range 2–3.5. These values were close to those reported in the literature for alumina-pillared clays and greater than those of zirconia-pillared clays, which indicates that the Al(*X*)Mt catalysts prepared could be a potential candidate for this reaction. A slight variation in the I/C ratio with alumina content was noted in our tested clays. However, Al(*X*)-PCH materials exhibited higher I/C ratios than with Al(*X*)-Mt, which were less than the zeolites and close to the common catalysts for this reaction.

The stability of the pillared clays has been investigated in the case of Al(6)-Mt by extending the time on stream at a reaction temperature of 350°C. The conversion and selectivity values decreased up to 12 h. This decrease was attributed to the formation of coke, which blocked the acid sites and favoured the cracking products. However, the Al(6)PCH catalyst exhibited a maximum conversion capacity of ~50% which decreased to 40% after 4 h of reaction and keeping steady for a period of 18 h on stream. These data could be related to the strength of acid sites and their stability under the experimental conditions.

CONCLUSIONS

Smectites intercalated with various quantities of Al species were reported and characterized, and further use of these precursors was successful in the synthesis of Al-PCH materials. The properties of these materials depended on the starting Al-intercalated precursors by means of the Al content in the precursors. Greater specific surface-area values were achieved and varied from 740 to 850 m^2/g with strong acid sites. Al(*X*)-PCH materials exhibited different activities towards n-C7 hydro-isomerization, which was reflected by different conversion and selectivity data with maximum values of 50% and 70% at a 300°C reaction temperature. The Al content in the pillared clays and their PCH derivatives affected the catalytic data and this could be related to the different strengths of the acid sites and the textural properties.

REFERENCES

Adams J.M. & McCabe R.W. (2006) Clay minerals as catalysts. Pp. 541–581 in: *Handbook of Clay Science* (F. Bergaya, B.K.G. Theng & G. Lagaly, editors). Elsevier, Amsterdam.

Ahenach J., Cool P. & Vansant E.F. (2000) Enhanced Brönsted acidity created upon Al-grafting of porous clay heterostructures. *Physical Chemistry and Chemical Physics*, **2**, 5750–5755.

Belver C., Aranda P., Martin-Luengo M.A. & Ruiz-Hitzky E. (2012) New silica/alumina–clay heterostructures: properties as acid catalysts. *Microporous and Mesoporous Materials*, **147**, 157–66.

Benjelloun M., Cool P., Van Der Voort P. & Vansant E.F. (2002) Template extraction from porous clay heterostructures: Influence on the porosity and the hydrothermal stability of the materials. *Physical Chemistry and Chemical Physics*, **4**, 2818–2823.

https://doi.org/10.1180/claymin.2017.052.4.09 Published online by Cambridge University Press

Borges R., Dutra L.M., Barison A. & Wypych F. (2016) MAS NMR and EPR study of structural changes in talc and montmorillonite induced by grinding. *Clay Minerals*, **51**, 69–80.

Breen C. (1991) Thermogravimetric study of the desorption of cyclohexylamine and pyridine from an acid-treated Wyoming bentonite. *Clay Minerals*, **28**, 473–486.

Breen C., Madejová J. & Komadel, P. (1995) Characterisation of moderately acid-treated, size-fractionated montmorillonites using IR and MAS NMR spectroscopy and thermal analysis. *Journal of Materials Chemistry*, **5**, 469–474.

Brindley G.W. & Hoffmann, R.W. (1962) Orientation and packing aliphatic chain molecules in montmorillonites. *Clays and Clay Minerals*, **9**, 546–556.

Carretero M.I. & Pozo M. (2009) Clay and non-clay minerals in the pharmaceutical industry: Part I. Excipients and medical applications. *Applied Clay Science*, **46**, 73–80.

Carretero M.I., Gomes CS.F. & Tateo F. (2006) Clays and human health. Pp. 717–742 in: *Handbook of Clay Science* (F. Bergaya, B.K.G. Theng & G. Lagaly, editors). Elsevier, Amsterdam.

Cecilia J.A., Garcia-Sancho C. & Franco F. (2013) Montmorillonite based porous clay heterostructures: Influence of Zr in the structure and acidic properties. *Microporous and Mesporous Materials*, **176**, 95–102.

Chmielarz L., Gil B., Kustrowski P., Piwowarska Z., Dudek B. & Michalik, M. (2009) Montmorillonite-based porous clay heterostructures (PCHs) intercalated with silica-titania pillars – synthesis and characterization. *Journal of Solid State Chemistry*, **182**, 1094–1104.

Chmielarz L., Piwowarska Z., Kustrowski P., Wegrzyn A., Gil B., Kowalczyk A., Dudek B., Dziembaj R. & Michalik M. (2011) Comparison study of titania pillared interlayered clays and porous clay heterostructures modified with copper and iron as catalysts of the DeNOx process. *Applied Clay Sciences*, **51**, 164–173.

Choy J.H., Yoon J.B., Jung H. & Park J.H. (2004) Zr K-Edge XAS and ^{29}Si MAS NMR studies on hexagonal mesoporous zirconium silicate. *Journal of Porous Materials*, **11**, 123–129.

Deldari H. (2005) Suitable catalysts for hydroisomerization of long-chain normal paraffins. *Applied Catalysis A: General*, **293**, 1–10.

Eswaramoorthi I., Geetha Bhavani A. & Lingappan N. (2003) Activity, selectivity and stability of Ni-Pt loaded zeolite-b and mordenite catalysts for hydroisomerisation of n-heptane. *Applied Catalysis A: General*, **253**, 469–486.

Galarneau A., Barodawalla A. & Pinnavaia J.T. (1995) Porous clay heterostructures formed by gallery-templated synthesis. *Nature*, **374**, 529–531.

Garea S.A., Mihal A.R., Vasile E. & Voicu G. (2014) Synthesis and characterization of porous clay heterostructures. *Revista de Chimie*, **65**, 640–656.

Ghadiri M., Chrzanowski W. & Rohanizadeh R. (2015) Biomedical applications of cationic clay minerals. *Royal Society of Chemistry Advances*, **5**, 29467–29481.

Ghanbari-Siahkali A., Philippou A., Dwyer J. & Anderson M.W. (2000) The acidity and catalytic activity of heteropoly acid on MCM-41 investigated by MAS NMR, FTIR and catalytic tests. *Applied Catalysis A: General*, **192**, 57–69.

González E., Rodríguez D., Huerta L. & Moronta, A. (2009) Isomerization of 1-Butene catalyzed by surfactant-modified, Al_2O_3-pillared clays. *Clays and Clay Minerals*, **7**, 383–391.

Hidalgo J.M., Zbuzek M., Cemy R. & Jisa P. (2014) Current uses and trends in catalytic isomerization, alkylation and etherification processes to improve gasoline quality. *Central European Journal of Chemistry*, **12**, 1–13.

Jones W. (1988) The structure and properties of pillared clays. *Catalysis Today*, **2**, 357–367.

Kloprogge J.T. (1998) Synthesis of smectites and porous pillared clay catalysts: A review. *Journal of Porous Materials*, **5**, 5–41.

Kloprogge J.T., Booy E., Jansen J.B.H. & Geus J.W. (1994) The effect of thermal treatment on the properties of hydroxy-Al and hydroxy-Ga pillared montmorillonite and beidellite. *Clay Minerals*, **29**, 153–167.

Kooli F. (2014a) Porous clay heterostructures (PCHs) from Al_{13}-intercalated and Al_{13}-pillared montmorillonites: Properties and heptane hydro-isomerization catalytic activity. *Microporous and Mesoporous Materials*, **184**, 184–192.

Kooli F. (2014b) Organo-bentonites with improved cetyltrimethylammonium contents. *Clay Minerals*, **49**, 683–692.

Kooli F. & Jones W. (1997) Systematic comparison of a saponite clay pillared with Al and Zr metal oxides. *Chemistry of Materials*, **9**, 2913–2920.

Kooli F., Bovey J. & Jones W. (1997) Dependence of the properties of Ti-pillared clays on the host matrix: a comparison of montmorillonite, saponite and rectorite pillared materials. *Journal of Materials Chemistry*, **7**, 153–158.

Kooli F., Khimyak Y.Z., Alshahateet S.F. & Chen F. (2005) Effect of the acid activation levels of montmorillonite clay on the cetyltrimethylammonium cations adsorption. *Langmuir*, **21**, 8717–8723.

Kooli F., Hian P.C., Weirong Q., Alshahateet S.F., Carriazo D., Martin C. & Rivers V. (2006a) Porous clay heterostructures from Al_{13} intercalated montmorillonites: synthesis and characterization. *Clay Science (supplement 2)*, **12**, 295–300.

https://doi.org/10.1180/claymin.2017.052.4.09 Published online by Cambridge University Press

Kooli F., Hian P.C., Weirong Q., Alshahateet S.F. & Fengxi C. (2006b) Effect of the acid-activated clays on the properties of porous clay heterostructures. *Journal of Porous Materials*, **13**, 319–324.

Kooli F., Yan L., Alshahateet S.F., Siril P. & Brown R. (2008) Effect of pillared clays on the hydroisomerization of *n*-heptane. *Catalysis Today*, **131**, 244–249.

Kooli F., Liu Y., Tan S.X. & Zheng J. (2014) Organoclays from alkaline-treated acid-activated clays. *Journal of Thermal Analysis and Calorimetry*, **115**, 1465–1475.

Kooli F., Liu Y., Hbaieb K. & Al-Faze R. (2016) Characterization and catalytic properties of porous clay heterostructures from zirconium intercalated clay and its pillared derivatives. *Microporous and Mesoporous Materials*, **226**, 482–492.

Liu, Y., Guan Y., Li C., Lian J., Gan G.J., Chew Lim E. & Kooli F. (2006a) Effect of ZnO additives and acid treatment on catalytic performance of $Pt/WO_3/ZrO_2$ for *n*-C7 hydroisomerization. *Journal of Catalysis*, **244**, 17–23.

Liu Y., Guo W., Zhao X.S., Lian J., Dou J. & Kooli F. (2006b) Zeolite beta catalysts for *n*-C7 hydroisomerization. *Journal of Porous Materials*, **13**, 359–364.

Lopez-Galindo A., Viseras C. & Cerezo P. (2007) Compositional, technical and safety specifications of clays to be used as pharmaceutical and cosmetic products. *Applied Clay Science*, **36**, 51–63.

Martinez-Oritz M.J., Fetter G., Dominguez J.M., Melo-Banda J.A. & Ramos-Gomez R. (2003) Catalytic hydrotreating of heavy vacuum gas oil on Al- and Ti-pillared clays prepared by conventional and microwave irradiation methods. *Microporous Mesoporous Materials*, **58**, 73–80.

Mokaya, R. & Jones W. (1995) Pillared clays and pillared acid-activated clays: a comparative-study of physical, acidic, and catalytic properties. *Journal of Catalysis*, **153**, 76–85.

Mokaya R., Jones W., Luan Z., Alba M.D. & Klinowski, J. (1996) Acidity and catalytic activity of the mesoporous aluminosilicate molecular sieve MCM-41. *Catalysis Letters*, **37**, 113–120.

Olaya A., Moreno S. & Molina R. (2009) Synthesis of pillared clays with aluminum by means of concentrated suspensions and microwave radiation. *Catalysis Communications*, **10**, 697–701.

Palkova H., Madejová J., Zimowska M., Bielanska E., Olejniczak Z., Litynska-Dobrzynska L. & Serwicka E.M. (2010) Laponite-derived porous clay heterostructures: I. Synthesis and physicochemical characterization. *Microporous and Mesoporous Materials*, **127**, 228–237.

Perdigón A.C., Li D., Pesquara C., Gonzalez F., Ortiz B., Aguado F. & Blanco C. (2013) Synthesis of porous clay heterostructures from high charge mica-type aluminosilicates. *Journal of Materials Chemistry A*, **1**, 1213–1219.

Pichowicz M. & Mokaya R. (2001) Porous clay heterostructures with enhanced acidity obtained from acid-activated clays. *Chemical Communications*, 2100–2101.

Polverejan M., Pauly T.R. & Pinnavaia T.J. (2000) Acidic porous clay heterostructures (PCH): Intragallery assembly of mesoporous silica in synthetic saponite clays. *Chemistry of Materials*, **2**, 2698–2704.

Rodriguez L.A.S., Figueiras A., Veiga F., Freitas R.M., Nunes L.C., Da Silva Filho E.C. & Leite C.M.S. (2013) The systems containing clays and clay minerals from modified drug release: a review. *Colloids Surface B Biointerfaces*, **103**, 642–651.

Schoonheydt R.A., Pinnavaia T.J., Lagaly G. & Gangas N. (1999) Pillared clays and pillared layered solids. *Pure and Applied Chemistry*, **71**, 2367–2371.

Tchinda A.J., Ngameni E., Kenfack I.T. & Walcarius A. (2009) One-step preparation of thiol-functionalized porous clay heterostructures: application to Hg(II) binding and characterization of mass transport issues. *Chemistry of Materials*, **21**, 4111–4121.

Thompson J.G. (1984) ^{29}Si and ^{27}Al nuclear magnetic resonance spectroscopy of 2:1 clay minerals. *Clay Minerals*, **19**, 229–236.

Wang Y., Zhang P., Wen K., Su X., Zhu J. & He H. (2016) A new insight into the compositional and structural control of porous clay heterostructures from the perspective of NMR and TEM. *Microporous and Mesoporous Materials*, **224**, 285–293.

Wilson J., Cuadros J. & Cressey G. (2004) An in situ time-resolved XRD-PSD investigation into Na-montmorillonite interlayer and particle rearrangement during dehydration. *Clays and Clay Minerals*, **52**, 180–191.

Yenfeng H., Xiangsheng W., Xinwen G., Silue L., Sheng H., Haibo S. & Liang B. (2005) Effects of channel structure and acidity of molecular sieves in hydroisomerization of *n*-octane over bi-functional catalysts. *Catalysis Letters*, **100**, 59–65.

Zimowska M., Litynska-Dobrzynska L., Olejniczak Z., Socha R.P., Gurgul J. & Tatka K. (2016) Alteration of the structure and surface composition of crystalline-amorphous porous clay heterostructures upon iron doping from metal-organic source. *Surface Interface Analysis*, **48**, 527–531.

https://doi.org/10.1180/claymin.2017.052.4.09 Published online by Cambridge University Press